

Evaluation of the NASA GISS Single-Column Model Simulated Clouds Using Combined Surface and Satellite Observations

AARON D. KENNEDY, XIQUAN DONG, AND BAIKE XI

Department of Atmospheric Sciences, University of North Dakota, Grand Forks, North Dakota

PATRICK MINNIS

NASA Langley Research Center, Hampton, Virginia

ANTHONY D. DEL GENIO

NASA Goddard Institute of Space Studies, New York, New York

AUDREY B. WOLF

Columbia University, New York, New York

MANDANA M. KHAIYER

Science Systems and Applications, Inc., Hampton, Virginia

(Manuscript received 21 July 2009, in final form 12 May 2010)

ABSTRACT

Three years of surface and Geostationary Operational Environmental Satellite (GOES) data from the Department of Energy Atmospheric Radiation Measurement (ARM) Southern Great Plains (SGP) site are used to evaluate the NASA GISS Single Column Model (SCM) simulated clouds from January 1999 to December 2001. The GOES-derived total cloud fractions for both 0.5° and 2.5° grid boxes are in excellent agreement with surface observations, suggesting that ARM point observations can represent large areal observations. Low (<2 km), middle (2–6 km), and high (>6 km) levels of cloud fractions, however, have negative biases as compared to the ARM results due to multilayer cloud scenes that can either mask lower cloud layers or cause misidentifications of cloud tops. Compared to the ARM observations, the SCM simulated most midlevel clouds, overestimated low clouds (4%), and underestimated total and high clouds by 7% and 15%, respectively. To examine the dependence of the modeled high and low clouds on the large-scale synoptic patterns, variables such as relative humidity (RH) and vertical pressure velocity (ω) from North American Regional Reanalysis (NARR) data are included. The successfully modeled and missed high clouds are primarily associated with a trough and ridge upstream of the ARM SGP, respectively. The PDFs of observed high and low occurrence as a function of RH reveal that high clouds have a Gaussian-like distribution with mode RH values of ~40%–50%, whereas low clouds have a gammalike distribution with the highest cloud probability occurring at RH ~75%–85%. The PDFs of modeled low clouds are similar to those observed; however, for high clouds the PDFs are shifted toward higher values of RH. This results in a negative bias for the modeled high clouds because many of the observed clouds occur at RH values below the SCM-specified stratiform parameterization threshold RH of 60%. Despite many similarities between PDFs derived from the NARR and ARM forcing datasets for RH and ω , differences do exist. This warrants further investigation of the forcing and reanalysis datasets.

Corresponding author address: Aaron Kennedy, Dept. of Atmospheric Sciences, Box 9006, University of North Dakota, 4149 Campus Rd., Grand Forks, ND 58202-9006.
E-mail: aaron.kennedy@und.edu

DOI: 10.1175/2010JCLI3353.1

© 2010 American Meteorological Society

1. Introduction

Clouds are one of the most important elements in the earth's hydrology and energy cycles, acting particularly through precipitation processes (Del Genio et al. 2005a) and the earth's radiation budget. Their treatment in weather forecast and climate models is a significant source of error and uncertainty (Gao and Li 2007; Cess et al. 1996; Randall et al. 2006). Although considerable uncertainty still surrounds cloud feedbacks in general circulation models (GCMs), one can assume that to reasonably simulate future climate, these models should be able to accurately reproduce the current climatology of all clouds at a given location. Due to the complexities of GCMs, the Single Column Model (SCM) approach was developed to evaluate parameterizations (Randall et al. 1996) and has been implemented by the Atmospheric Radiation Measurement (ARM) program (Ackerman and Stokes 2003) to improve the representation of clouds and radiation in GCMs using long-term surface observations (Klein and Del Genio 2006).

SCM versions of GCMs typically have been used to simulate the atmosphere over limited time periods, driven by field experiment data or enhanced soundings during intensive observing periods (IOPs; see the 2005 special issue of *J. Geophys. Res.*, volume 110, issue D15). These exercises have proven difficult to interpret because model–data discrepancies can be due to inaccurate large-scale advective forcing, inaccurate model physics, or problems with the cloud data, and instantaneous model errors may not be climatically representative or diagnostic of problems with the model's cloud feedback (Del Genio et al. 2005b). Therefore, it is necessary to use a longer time series to have a statistically meaningful comparison.

Compared to observations from the International Satellite Cloud Climatology Project (ISCCP) (Rossow and Schiffer 1999) and the Clouds and the Earth's Radiant Energy System (CERES) (Wielicki et al. 1996; Minnis et al. 2010a, manuscript submitted to *IEEE Trans. Geosci. Remote Sens.*), Zhang et al. (2005) found that the majority of GCMs only simulated 30%–40% of observed midlatitude midlevel-top clouds and half of the GCMs underestimated low-level-top clouds, however, not at a statistically significant level. Limitations in the passive satellite data prevented a thorough analysis of high, optically thin clouds due to the observed differences between the CERES and ISCCP datasets.

To ensure that climate models reliably represent clouds, the parameterizations of cloud–radiation–precipitation interactions and the associated heating and other feedbacks in the models should faithfully represent what is found in nature. Therefore, the time-dependent frequency distributions of cloud properties from the model

should also be compared to those derived from observations. Ultimately, improved cloud parameterizations can only result from an integrated analysis of all available datasets, including long-term surface and satellite observations, SCMs, and reanalyses.

To provide a much-needed source of long-term cloud–radiation data for evaluating model parameterizations, the ARM program established the Southern Great Plains (SGP) site, centered near Lamont, Oklahoma, in 1993. ARM has also included satellite observations to determine cloud and radiative properties (Minnis et al. 1995, 2001) to complement the surface data, provide large-scale averages, and bound the radiation budget at the top of the atmosphere (TOA). In addition to the surface and satellite measurements, Xie et al. (2004) developed the continuous forcing product (1999–2001) over the SGP site. This product is often of a quality comparable to that from the Intensive Observing Periods (IOPs) and has the advantage of being available for driving SCMs over long periods (Del Genio et al. 2005b).

This paper reports on a continuous period of long-term surface and satellite observations, SCM simulations, and their association with large-scale synoptic patterns and variables provided by the North American Regional Reanalysis (NARR) over the ARM SGP site. Although the evaluation of an individual SCM driven by a forcing dataset at one location may have limited practical usage, the ARM SGP site is representative of a continental climate in the midlatitudes. The paper is formatted as follows. Section 2 gives a brief description of the different datasets used in this study. In section 3, satellite- and surface-observed clouds are compared to the SCM simulations on hourly, monthly, and seasonal time scales. SCM performance is investigated within section 4 with the aid of large-scale parameters obtained from NARR and ARM forcing. Pertinent conclusions are summarized along with plans for future work in the final section.

2. Datasets

Surface, satellite, ARM continuous forcing, and NARR reanalysis datasets have been collected at the ARM SGP site during the period 1999–2001 for this study. Because the ARM continuous forcing is required to run the GISS SCM and is only available during 1999–2001, model results are compared with both surface and satellite observations for this 3-yr period. Both surface and satellite datasets are averaged into hourly means to match the SCM hourly temporal resolution although their spatial resolutions are different. However, as demonstrated in the Xi et al. (2010) study and supported in this one, cloud fraction (CF) is independent of temporal resolution and spatial scale. Long-term CFs derived from

different temporal resolutions of surface observations can represent the areal CFs averaged from different GOES grid boxes provided there are enough samples and that clouds occur with equal frequency throughout the domain of interest.

a. Surface observations

The Department of Energy (DOE) ARM 35-GHz Millimeter Wavelength Cloud Radar (MMCR) has a minimum detectable reflectivity factor (Z) of -55 dBZ at 1 km and -35 dBZ at 10 km (Moran et al. 1998). The MMCR operates at a wavelength of 8 mm in a vertically pointing mode and provides continuous profiles of radar reflectivity from hydrometeors moving through the radar field of view (FOV), allowing the identification of clear and cloudy conditions. The beamwidth is 0.2° , which results in a horizontal resolution of ~ 40 m at 12 km AGL. Cloud-top height (H_{top}) is derived from MMCR reflectivity profiles, with an uncertainty of 90 m. The lowest cloud-base height (H_{base}) is derived from a composite of Belfort laser ceilometer, Micropulse lidar (MPL), and MMCR data (Clothiaux et al. 2000). Inclusion of the lidar allows for the filtering of insects, which produce a significant reflectivity during the spring and summer seasons over the ARM SGP site. Another source of error in the cloud radar observations is attenuation during heavy precipitation events, which leads to underestimated cloud-top heights. To mitigate this issue, only times are considered when MPL and MMCR cloud-base estimates are available during dry or lightly precipitating periods. This is expected to cause a negligible amount of negative bias to cloud fractions derived for all levels; only 0.4% of all 5-min samples were filtered out for this dataset.

The cloud fraction (CF), derived from the upward-looking narrow FOV radar–lidar pair of measurements, is simply the percentage of returns that are cloudy within a specified sampling time period, that is, the ratio of the number of 5-min samples when clouds were detected to the total number of samples when both radar and lidar–ceilometer instruments were working.

b. Satellite observations

The satellite cloud products (Minnis et al. 2001) were retrieved using algorithms developed for the NASA Clouds and the Earth's Radiant Energy System project. Cloud properties were retrieved from half-hourly, 4-km 0.65-, 3.9-, 10.8- (infrared, IR), and 12.0- μm radiances taken by *GOES-8*. Cloudy pixels were identified using an adaptation of the method described by Minnis et al. (2008). The visible infrared solar-infrared split-window technique (VISST) was applied during daytime (solar

zenith angle $< 82^\circ$) and the solar-infrared infrared split-window technique (SIST) was used at night (solar zenith angle $> 82^\circ$) to derive cloud properties for those pixels (Minnis et al. 2010b, manuscript submitted to *IEEE Trans. Geosci. Remote Sens.*). The areal fraction of clouds (or the amount when present, AWP) is the ratio of the number of pixels classified as cloudy to the total number of pixels within a specified area ($0.5^\circ \times 0.5^\circ$ in this study). The primary technique for determining the effective cloud height (H_{eff}) is to estimate the effective cloud temperature (T_{eff}) based on the 10.8- μm radiance adjusted to account for cloud semitransparency first, and then to define H_{eff} as the lowest altitude having T_{eff} from a vertical temperature profile.

The profile is constructed in three parts. The Rapid Update Cycle (RUC) numerical weather analysis model (Benjamin et al. 2004) profile is used for pressures $p < 500$ hPa. The profile for $p > 700$ hPa is specified using a -7.1 K km^{-1} lapse rate anchored to the 24-h running mean surface temperature from the RUC, while a linearly weighted blend of the RUC and lapse rate is used for intermediate pressures. Dong et al. (2008) demonstrated that the lapse rate approach is more reliable for assigning cloud-top height from T_{eff} for boundary layer clouds than using the soundings from either sparse radiosonde measurements or numerical weather analyses. This study uses the gridded layer-averaged *GOES-8* AWP (Palikonda et al. 2006; data available online at <http://www-angler.larc.nasa.gov/>). According to the retrieved H_{eff} , the *GOES*-derived clouds can be classified as low (< 2 km), middle (2–6 km), and high (> 6 km) clouds. Total cloud coverage is simply the sum of the low, middle, and high AWP determined from the *GOES* data.

c. NASA GISS SCM

The model analysis in this paper uses an archived run of the NASA GISS SCM that is identical to the one described in Del Genio et al. (2005a,b). The model is based on the SI2000 version of the GCM, but with cloud and convection physics updates described in Del Genio et al. (2005a). The SCM has 35 vertical layers and an implied horizontal resolution of $2^\circ \times 2.5^\circ$, corresponding to a grid box of approximately 220 km square at the SGP. The continuous forcing driving this SCM run uses constrained variable analysis with RUC-2 hourly analyses as the background field (Zhang et al. 2001; Xie et al. 2004). These hourly analyses are constrained by ARM surface and *GOES-8* satellite observations to balance observed mass, momentum, heat, and moisture budgets within the column. The forcing represents a circular area approximately 180 km in radius from the central facility at ARM SGP. This is approximately 2.2 times that of the

TABLE 1. Resolutions of the various datasets used in this publication.

| Dataset | Temporal | Areal | Height |
|------------------------|------------|-------------------|-------------------|
| ARM SGP MMCR | 5 min | <60 m (0.2° beam) | 90 m |
| GOES VISST | ~15–30 min | 0.5° × 0.5° | 3 levels |
| NASA GISS SCM | 1 h | 2.0° × 2.5° | 35 levels, ~25 mb |
| NARR reanalysis | 3 h | 0.3° × 0.3° | 29 levels, ~25 mb |
| ARM continuous forcing | 1 h | 180-km radius | 37 levels, ~25 mb |

implied resolution. The model is run hourly from the observed advective temperature and moisture tendencies, and is reinitialized at the beginning of each day to remove climatic drift (Del Genio et al. 2005a).

The SCM predicts cloud water but uses a RH-based scheme to diagnose the large-scale cloud fraction (Sundqvist et al. 1989; Del Genio et al. 1996), which requires a tunable threshold relative humidity parameter, U_{00} . Commonly set around 60%, stratiform clouds are not allowed to occur below this value. Above this threshold, cloud amount (fraction) is assumed to increase with grid-box mean RH. The U_{00} is held constant globally and vertically, and only varies (relative to saturation over liquid water) when temperatures are below -35°C to account for the differences between saturation vapor pressure over ice rather water. For this reason and also because the convective scheme separately diagnoses a convective cloud cover, the SCM can occasionally create clouds at values below the prescribed threshold (Del Genio et al. 1996). The convective scheme uses mass flux and is closed by moving enough mass to neutralize cloud-base instability (Del Genio and Yao 1993). This scheme allows for up to two convective cloud tops (such as cumulus and cumulonimbus) and cirrus anvils by detraining water vapor condensate from the convective scheme into the grid box, where the subsequent evolution is handled by the stratiform scheme. SCM cloud fractions are diagnosed with an International Satellite Cloud Climatology Project (ISCCP) simulator that uses a random-maximum assumption for cloud overlap (Klein and Jakob 1999).

d. NARR

The National Centers for Environmental Prediction (NCEP) North American Regional Reanalysis (NARR) (Mesinger et al. 2006) is a long-term (1979–2007) climate dataset with 3-h temporal, 32-km horizontal, and 45-layer vertical resolutions over the North American domain. It contains outputs of many atmospheric variables and fluxes and is nicely suited for diagnosis of synoptic and mesoscale conditions over the ARM SGP site. NARR uses the operational NCEP Eta Model and its three-dimensional variational data assimilation (3DVAR) technique on a wide variety of observation platforms.

3. Evaluation of the NASA GISS SCM simulations

a. Methodology

Although the ARM radar–lidar observations provide the most reliable vertical distributions for verifying the GCM simulations, large-scale satellite data are critical for evaluating GCM simulated spatial distributions of clouds because they provide a means to account for the scale differences between the SCM and surface site. Comparisons between the ground- and satellite-based observations must be conducted carefully because of significant spatial and temporal differences between the two different observing platforms. Xi et al. (2010) have shown that there is excellent agreement in monthly mean CFs determined from 10 years of surface and GOES data. The CF is independent of temporal resolution and spatial scales, at least up to the size of a 2.5° grid box, providing there are enough samples. Cloud frequency of occurrence increases and AWP decreases with increasing averaging time and spatial scale.

The temporal, spatial, and vertical resolutions of the surface radar–lidar and GOES observations and SCM simulations are listed in Table 1. To have the same temporal resolution for the three datasets, both surface and GOES datasets have been averaged into hourly means to match the SCM hourly outputs. Since GOES can provide only three levels (low, middle, and high) of clouds, both surface (90-m resolution) and SCM (~25-hPa resolution) vertical distributions of clouds have been binned into those three levels to make a reasonable comparison. Although this definition is different from the more widely used ISCCP definition of cloud heights (high: <440 hPa, middle: 440–680 hPa, and low: >680 hPa), the differences between the two definitions are minimal for most calculations of CF. For spatial resolution, the $0.5^{\circ} \times 0.5^{\circ}$ grid box of the GOES observations has been extended into a $2^{\circ} \times 2.5^{\circ}$ grid box to match the SCM domain. Figure 1 shows an enlarged 2.5° grid box, including the percentages of the area from each 0.5° grid box.

Satellite observations may include several error sources that can significantly impact the derived AWP. In particular, observational noise or retrieval errors can lead to positively biased cloud frequencies for the 0.5° grid box because more clouds occur for very small

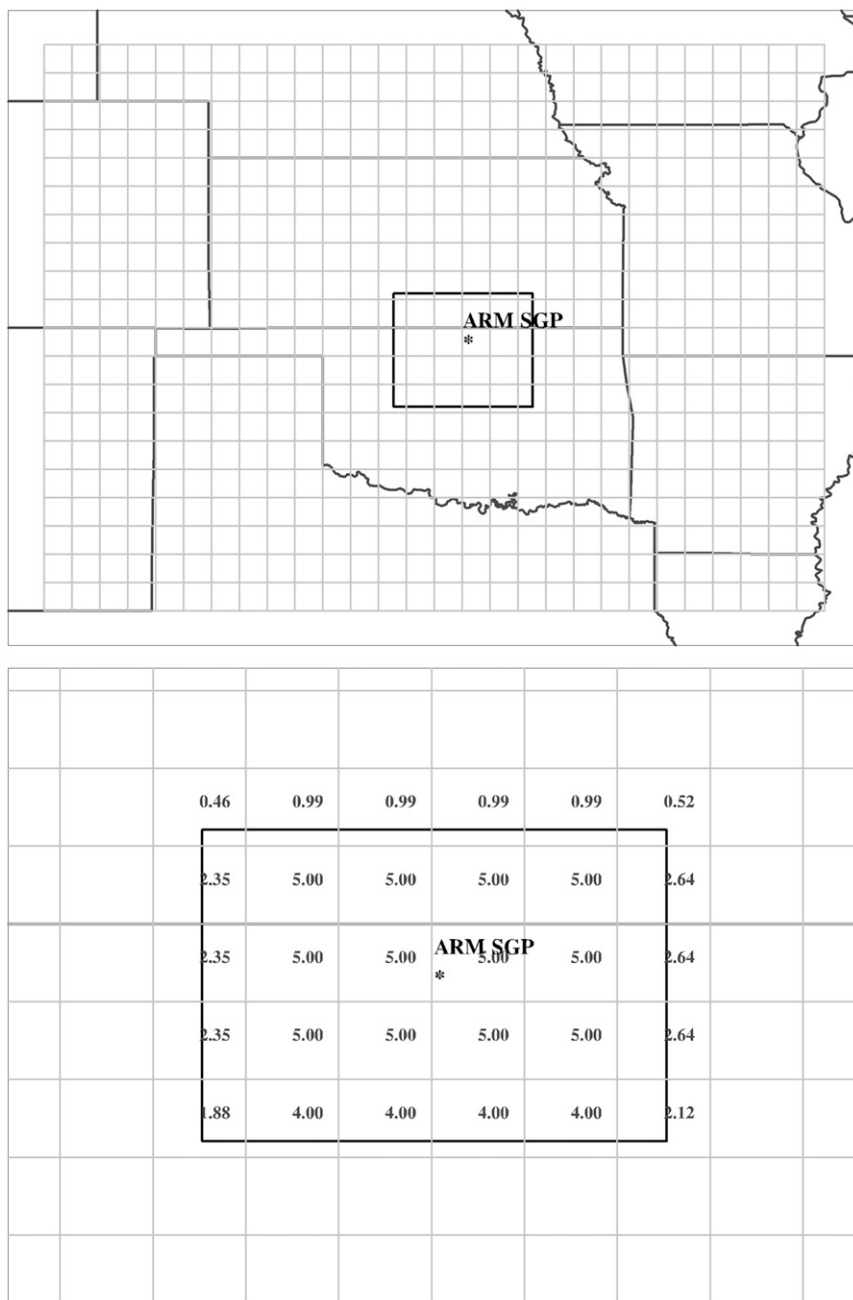


FIG. 1. (top) Domain for this study. The thick box is the $2^{\circ} \times 2.5^{\circ}$ SCM domain centered on the ARM SGP CF site denoted by the star. The finer grid represents the $0.5^{\circ} \times 0.5^{\circ}$ GOES cloud product used in this study. (bottom) An enlarged $2^{\circ} \times 2.5^{\circ}$ grid box that includes the percentages of area from each 0.5° box that contributed to the $2^{\circ} \times 2.5^{\circ}$ GOES average.

AWPs (<5%). Figure 2a illustrates the hit rate (fraction of hours during which satellite and radar observations agree) as a function of the instantaneous GOES AWP threshold used here to discriminate between cloudy and clear scenes. The impact of noise or retrieval errors is easily seen for low clouds where their hit rate increases

to a maximum at ~10% AWP and then is asymptotic to a hit rate of 0.8. This in turn impacts the total cloud hit rate and suggests that for the best agreement between radar and satellite observations, a threshold AWP must be set to discriminate between cloudy and clear scenes on an hour-to-hour basis. Other than a minimum below

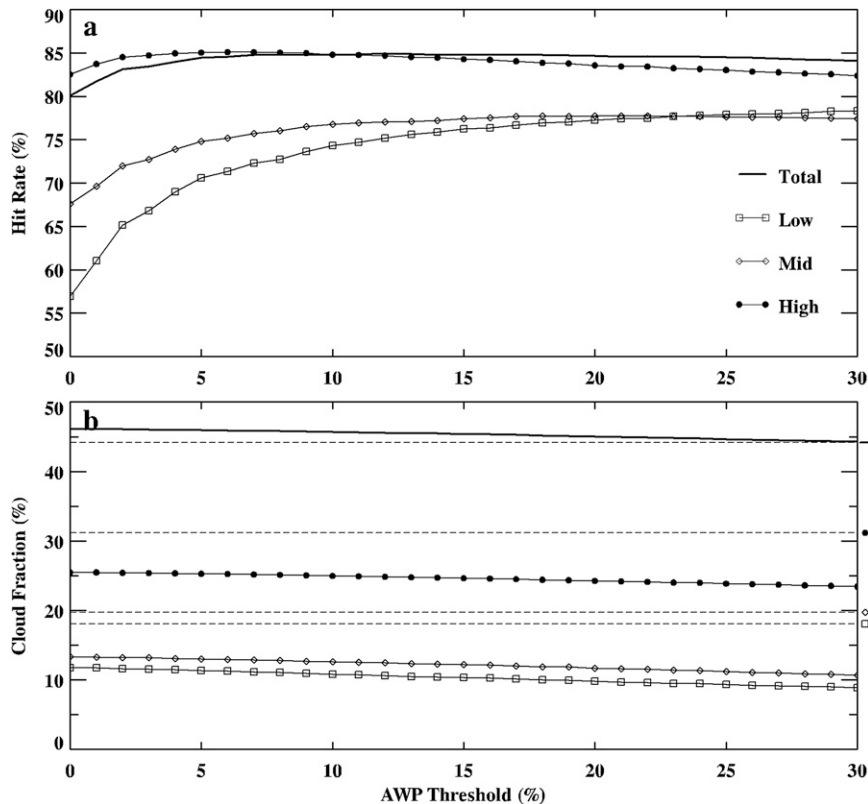


FIG. 2. Dependence of (a) hit rate and (b) cloud fraction on the AWP threshold for $0.5^\circ \times 0.5^\circ$ satellite observations. An AWP is used to discriminate cloudy ($\geq 5\%$) and clear scenes ($< 5\%$) in this study. Dashed lines in (b) are the radar–lidar observed cloud fractions with the relevant layer indicated by the symbol along the right axis.

2%, the hit rate slowly decreases for high clouds, which indicates that setting a threshold too high would arbitrarily classify correct retrievals of clouds by the satellite as clear. Except for optically thin cirrus, satellites should detect most high clouds. Figure 2b demonstrates the impact of the prescribed AWP thresholds on the GOES-derived CF. Small AWP thresholds alter the derived cloud fractions by a negligible amount (less than 1%). To filter out GOES observational noise and/or retrieval errors and to keep more cloud samples within the SCM domain, a threshold of 5% GOES AWP was used to discriminate cloudy ($\geq 5\%$) and clear ($< 5\%$) scenes in this study.

To further investigate the 5% threshold, consider Fig. 3, which illustrates the frequencies of GOES-observed (before applying the 5% threshold) and SCM-simulated AWP. The distributions of the GOES AWP is characterized by being bimodal for high clouds and exponentially decreasing for the low- and midlevel clouds. Note that the AWP within the first bin of all three levels are less than 5% and have been filtered out in this study. Even if some of these scenes are realistic, the radiative impact of such a small cloud coverage is probably minimal

on climatic scales. Despite the large peaks in the first bin in Fig. 3, the distributions are consistent with the Zhang (2003) study, which explored GOES AWP distributions over a $9.5^\circ \times 13.5^\circ$ area centered on the ARM SGP during a summer month. Modeled three-level cloud fractions peak at large AWP ($> 85\%$), while others are nearly equally distributed from 5% to 85%. This is most likely caused internally within the SCM cloud parameterization scheme when volumetric cloud fraction is converted into the horizontal scale.

b. Cloud fraction and frequency

For the GOES results, the cloudy frequency of occurrence (FREQ) is taken to be 0 for $\text{AWP} < 5\%$ and 1 when $\text{AWP} \geq 5\%$. The monthly averaged AWP is the average of all hourly AWP ($> 5\%$) and represents the averaged cloud amount when clouds are present. The average FREQ (probability of cloud occurrence) is the ratio of the number of times $\text{AWP} > 5\%$ to the total number of satellite observations during that month. Finally, the monthly mean CF (or coverage/amount), following Warren et al. (1984) and Hogan et al. (2001), is defined as the product

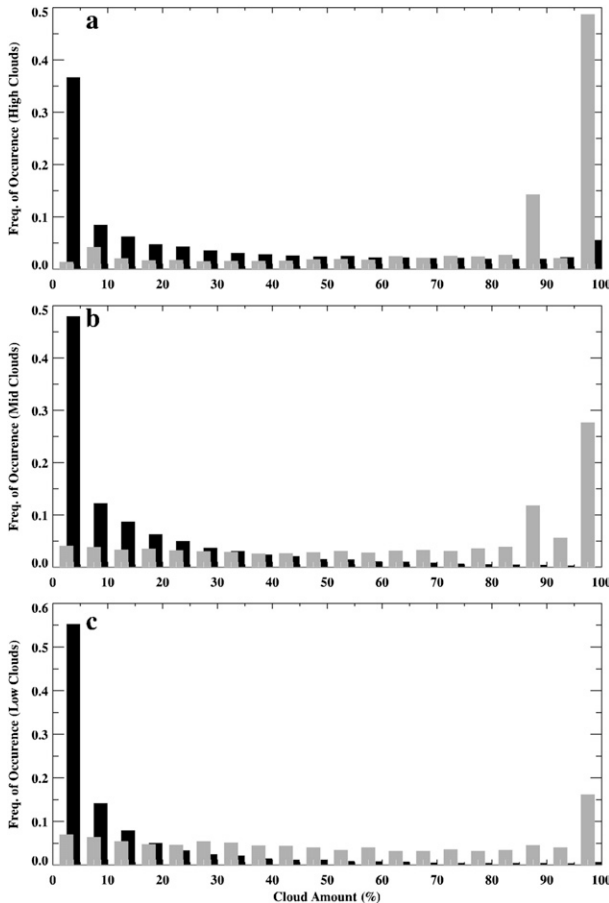


FIG. 3. Frequency distributions of AWP for (a) high, (b) middle, and (c) low clouds derived from GOES observations (black, before applying a threshold of 5%) and SCM simulations (gray).

of the averaged instantaneous AWP and FREQ. This is equivalent to the CF derived by the radar–lidar observations if clouds occur uniformly over the domain.

1) DIURNAL VARIATION OF CLOUD FRACTION

The diurnal variations of hourly mean total and three-level CFs are illustrated in Fig. 4. The diurnal cycles are plotted in UTC (SGP local time = UTC – 6 h) because the SCM was reinitiated at 0000 UTC every day with no spinup period. For surface observations, diurnal variations primarily occur for low clouds, which are typically subject to mesoscale or microscale forcing with the sunrise/sunset. There are more low-level clouds in the morning than during the afternoon. Very little variability occurs for clouds above 6 km that are more often tied to large-scale forcing independent of the diurnal cycle. Other than anvil cirrus clouds due to afternoon/evening thunderstorms, high-level clouds are often associated with the large-scale forcing, such as ascent with baroclinic waves.

For GOES-derived CFs, there is no strong diurnal variation for total clouds, but there is a significant drop for high clouds and an increase in both low and middle clouds around sunrise (~ 1200 – 1300 UTC in Fig. 4). This is primarily caused by the effect of multilayered clouds on the different retrieval algorithms used for day and night. The increased low- and midlevel CF during daytime is mainly due to the fact that high, thin cirrus over low clouds only slightly diminishes the IR brightness temperature T_{IR} , but the visible channel indicates that the cloud is optically thick. The net result is that the VISST assumes that the T_{eff} is essentially the same as T_{IR} . Thus, the VISST retrievals for thin-over-thick multilayered cloud systems yield a low- or midlevel cloud depending on the altitude of the lower cloud and the optical thickness of the upper-level cloud. If the upper-level cloud has an optical depth greater than ~ 3 or so, the cloud is interpreted as a high cloud and the lower cloud is undetected. Even in single-layered cirrus cases, the cloud height is underestimated (Smith et al. 2008) because the cirrus optical depth is overestimated (Min et al. 2004).

At night, however, the SIST is relatively insensitive to the presence of a low-level cloud underneath a thin high cloud because the surface and low-cloud temperatures typically differ by only a few degrees. Thus, the upper-level cloud is detected as being semitransparent and T_{eff} differs significantly from T_{IR} and a relatively accurate high-cloud altitude results for both single (Smith et al. 2008) and multilayered clouds (Xi et al. 2010). The low clouds underneath the cirrus are not detected. These algorithmic effects result in the high-cloud CF decreasing from nighttime to daytime, which corresponds to an apparent increase for low- and midlevel clouds. The low- and midlevel CFs are always less than the values from the radar because of the screening effect of the high clouds.

The SCM simulated clouds monotonically increase from 0000 UTC to early morning (~ 1200 UTC) for total and all three-level clouds, as shown in Fig. 4. The daytime (1200–2400 UTC) minus nighttime (0000–1200 UTC) CF differences vary by 28%–37%, depending on the level. Although other issues cannot be completely ruled out, the culprit for this steady increase in CF is mainly due to the 0000 UTC daily initialization for the model. As might be expected, this model spinup time (~ 12 h as shown in Fig. 4) would introduce a negative bias to all cloud fraction calculations. Therefore, all CFs derived from surface, GOES, and SCM datasets are based only upon the 1200–2400 UTC time period in this study.

2) SEASONAL VARIATION OF CLOUD FRACTION AND FREQUENCY

The monthly variations of total, high, middle, and low cloud fractions and frequencies derived from surface

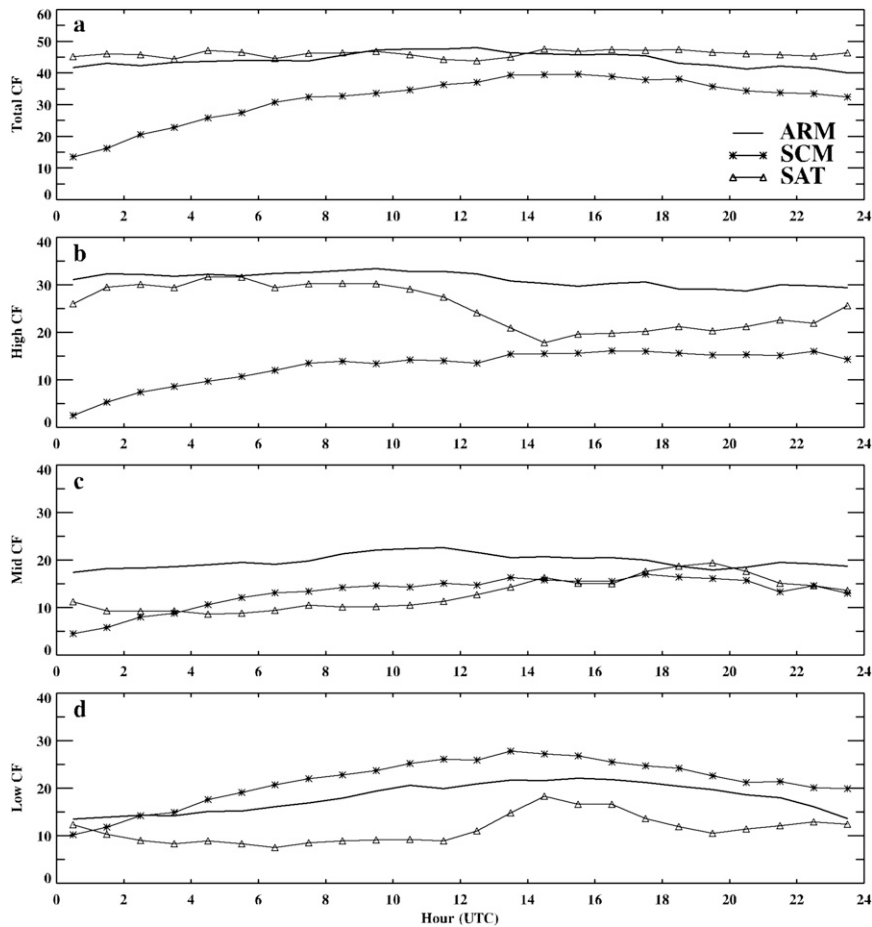


FIG. 4. Hourly mean cloud fraction for (a) total and (b) high-, (c) middle-, and (d) low-level clouds derived from the surface radar–lidar, $0.5^{\circ} \times 0.5^{\circ}$ grid box of GOES observations, and SCM simulations (from the ISSCP simulator with the random-maximum assumption of cloud overlap) at ARM SGP, 1999–2001.

radar–lidar, 0.5° and 2.5° grid boxes of GOES observations, and SCM simulations at the SGP site during the 3-yr period are illustrated in Fig. 5. Their corresponding annual means are summarized in Table 2. Both surface and GOES-derived total CFs agree very well in the general trend and magnitude, with almost identical annual means. They both peak during the January–March period, have a second peak in June, followed by a significant drop into July, and increase again from summer to winter. The monthly variations of the three-level CFs basically follow the total CF trend with minor variations. Although the GOES-derived high CF is less than that from the surface, the high-cloud frequency agrees well with surface observations suggesting that at least part of the high-cloud cover is correctly identified whenever high clouds occur during the daytime. Middle and low CFs are less than the surface observations throughout the year except for the July–August period. This is understandable because some of the middle and low clouds

are masked by upper-level clouds. The fact that some of the low and midlevel clouds are actually misidentified high clouds, as discussed above, is reinforced by their greater frequencies of occurrence as seen by the satellite. Although these comparisons are based on a 3-yr dataset, it is concluded that they are typical because the seasonal variations of clouds in this study are similar to other studies that used longer time series (Dong et al. 2006; Xi et al. 2010).

Despite being consistently less than observations, the monthly variations of SCM-simulated total and three-level clouds undergo seasonal changes that are somewhat similar to those observed from the surface and satellite with one exception. The SCM midlevel CF maximum is several months out of phase with the others, but still corresponds with a local maximum in the observations. As seen in both Figs. 4 and 5, the SCM simulates significantly fewer clouds overall ($\sim 10\%$) than detected by the observations. Investigation of individual

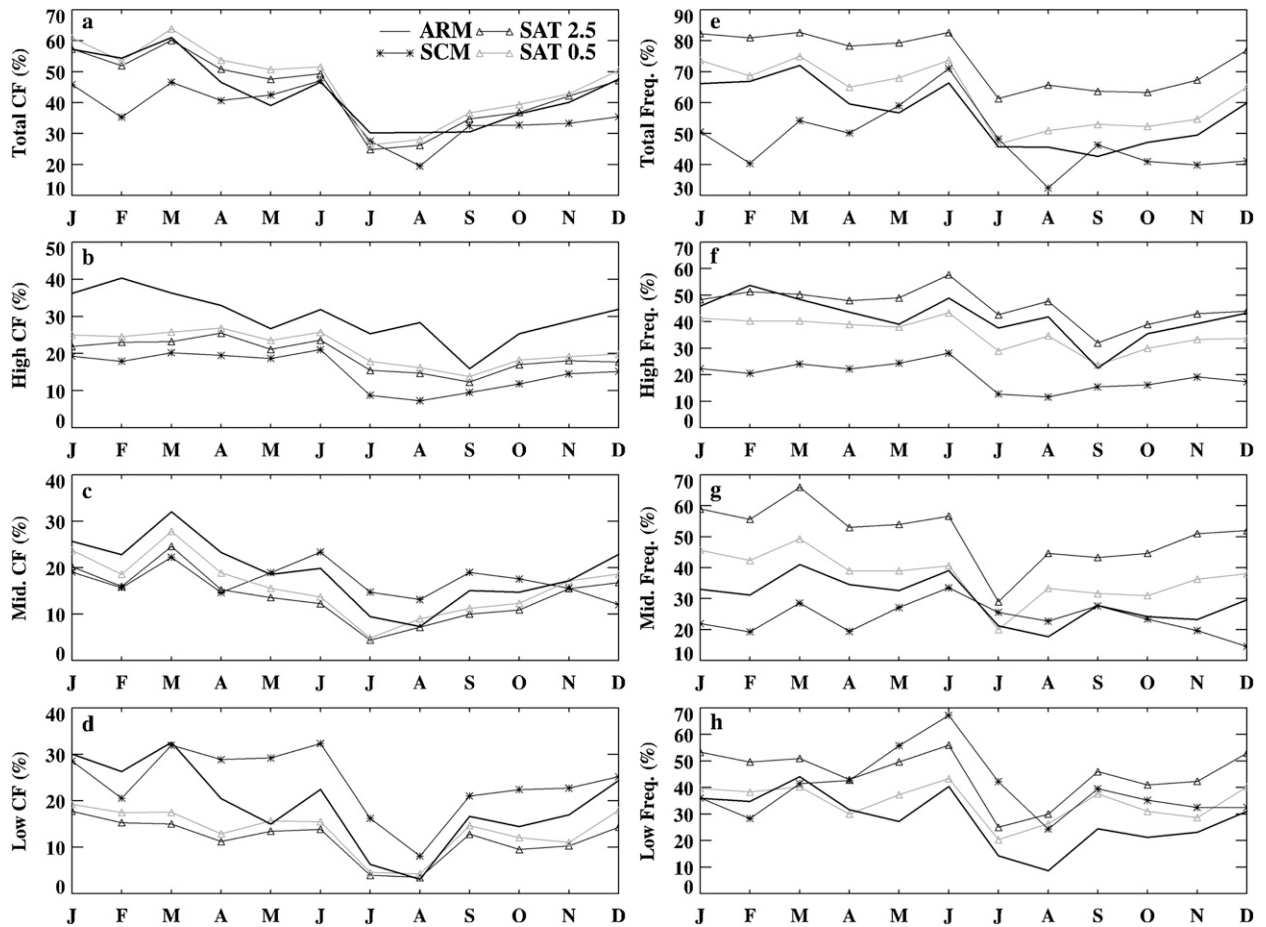


FIG. 5. (left) Monthly mean cloud fraction and (right) frequency of occurrence for total and high-, middle-, and low-level clouds derived from surface radar–lidar and $0.5^{\circ} \times 0.5^{\circ}$ and $2^{\circ} \times 2.5^{\circ}$ grid boxes of GOES observations and SCM simulations at ARM SGP, 1999–2001.

layers reveals that the SCM underestimated high clouds but simulated most of the middle and low clouds compared to the surface and GOES observations.

The monthly variations of cloud frequencies are nearly the same as their CF counterparts but with relatively large values. As expected, the observed cloud frequencies are greater for the large grid box (2.5°) than for the small grid box (0.5°) and ARM surface observations; that is, the cloud frequencies increase with larger spatial scales. For high clouds, the 0.5° grid box of GOES- and radar-observed cloud frequencies are nearly equivalent, which suggests that on the order of an hour radar observations are a good approximation for a 0.5° grid box of satellite observations. The SCM simulated cloud frequencies are lower than the observed ones except for low clouds. For high clouds, the SCM frequency is nearly the same as its CF (19% versus 15%), which indicates that the model simulated either clear skies or scenes with large AWP. This argument is also supported by Fig. 3a.

Table 2 summarizes the 3-yr-averaged cloud fractions and frequencies for total and three-level clouds. The percentages of surface and GOES observations and SCM simulations used are 84%, 93%, and 100% of all possible data during the 3-yr period, respectively. As listed in Table 2, the GOES-derived total CFs from both 0.5° and 2.5° grid boxes are in excellent agreement with surface observations, while for individual cloud layers the limitation

TABLE 2. Averaged cloud fraction (CF) and frequency of occurrence (FREQ) from observations and model simulations during the period 1999–2001. All numbers are given in percentages.

| | CF/FREQ | | | |
|--------|-------------|-----------------------|-----------------------|-----------------------|
| | Radar–lidar | SAT (0.5°) | SAT (2.5°) | SCM (2.5°) |
| Total | 44/57 | 46/62 | 44/74 | 37/48 |
| High | 30/42 | 21/36 | 19/46 | 15/19 |
| Middle | 20/30 | 16/38 | 14/51 | 17/24 |
| Low | 20/29 | 14/35 | 12/45 | 24/40 |

of GOES satellite observations is apparent. All three individual layers of CF are less than the surface results. This discrepancy can be explained as follows: 1) the difficulty of cloud-base detection by passive sensing satellites, 2) missed or underestimated H_{eff} for optically thin cirrus clouds, 3) missed low-level clouds when optically thick cloud layers are present above, and 4) the limitation of nighttime retrievals without visible channels. Despite the difficulties in detecting these lower clouds, the good agreement of the total and high cloud categories for satellite and radar observations provides strong evidence that the long-term observations of CF at the ARM SGP site are representative of a large grid box of satellite observations. It is expected that the 0.5° GOES-derived CFs should be more representative of the surface-retrieved CFs than the larger-scale averages. Thus, since the total CF for the smaller box is 2% greater than that for the 2.5° box, it can be assumed that differences in cloud cover less than $\sim 2\%$ between the large-scale SCM and the surface site are insignificant.

3) VERTICAL AND MONTHLY DISTRIBUTION OF CLOUD FRACTIONS

To evaluate the vertical and monthly distribution of SCM simulated clouds, ARM MMCR data were binned into the same vertical resolution of the model (~ 25 hPa). Figure 6 shows the monthly mean time–height series of cloud fractions derived from ARM MMCR observations and simulated by the GISS SCM over the ARM SGP, as well as their differences during the 3-yr period. The observed cloud fraction has a bimodal distribution with a higher peak at ~ 300 hPa and a lower one near the top of the boundary layer at ~ 850 hPa. The largest cloud fractions occur during the late winter and early spring seasons when baroclinic wave activity is common over the ARM SGP site. High-cloud fraction also varies somewhat with the fall and rise of the tropopause heights by season due to the thermal thickness of the atmosphere.

The simulated CFs in Fig. 6b differ substantially from the observed values. In addition to the aforementioned lack of high clouds and excess of low clouds, several specific seasonal errors exist: 1) the observed peak at 300 hPa during late winter is missing in the SCM and 2) the overproduction of boundary layer clouds is most prominent in the lowest couple of model layers during late winter and early spring with values of 5%–10% over the observed CF. In fact, if these layers were ignored, the SCM would have a negative bias for clouds near the top of the PBL. Given that the model uses a stratiform scheme that is based on grid-box mean RH, this is consistent with time periods of high RH in the boundary layer.

The time–height series of modeled cloud fractions in Fig. 6 raises the following question: are the consistent

differences between the MMCR and SCM-simulated clouds caused by the model cloud parameterizations, by clouds that are forced on a scale irresolvable by the model and its forcing, or by errors in the ARM continuous forcing? The cloud parameterizations within the NASA GISS SCM use large-scale variables, such as RH and cumulus mass flux, to predict clouds. Changes in the model–observation cloud with season and height suggest that either the relationships of cloud fraction with these parameters vary seasonally or advective forcing is variable by season. High clouds, for example, are underestimated regardless of season, and very few are produced during the summer.

One possible cause of a consistent negative bias for clouds is the lack of consideration for condensate advection in SCMs. This is a difficult problem to address because observations of condensate advection are limited. While advection is most important for high clouds, which are the principal deficiency for the model simulation in this paper, it is also true that ice sedimentation limits this problem to an extent. Klein and Jakob (1999) performed a sensitivity study for the European Centre for Medium-Range Weather Forecasts related to this problem and found that the inclusion of advection had minimal impact (3%) on the simulation of cloud fraction. Given that this percentage is much smaller than the biases for the high-cloud fraction in this paper, it is concluded that condensate advection cannot be the predominant issue.

This bias could be explained by a variety of other mechanisms, however. Climatologically, Oklahoma is dominated by large-scale ridging during summer. With plentiful subsidence and the lack of baroclinic waves to transport moisture to the upper atmosphere, its RH is lower than during other seasons. Considering that the model uses RH to simulate stratiform clouds, it is not difficult to fathom less cloud cover being simulated during the summer months. Another plausible explanation may be that the model cannot simulate an adequate amount of subgrid-scale convection, thereby generating fewer cirrus anvils from convective clouds during the summer. The consistent negative bias of high clouds, however, suggests that an issue exists regardless of cloud forcing. To partially answer the questions and test the various hypotheses, the association of observed and modeled clouds with NARR-derived synoptic patterns and ARM continuous forcing is explored in the following sections.

4. Association of the observed and modeled clouds with large-scale synoptic pattern

To match the temporal resolution of the NARR dataset, the radar observations and SCM simulations were reduced to 3-hourly time steps for this portion of the study. For simplicity, each time step is classified as either

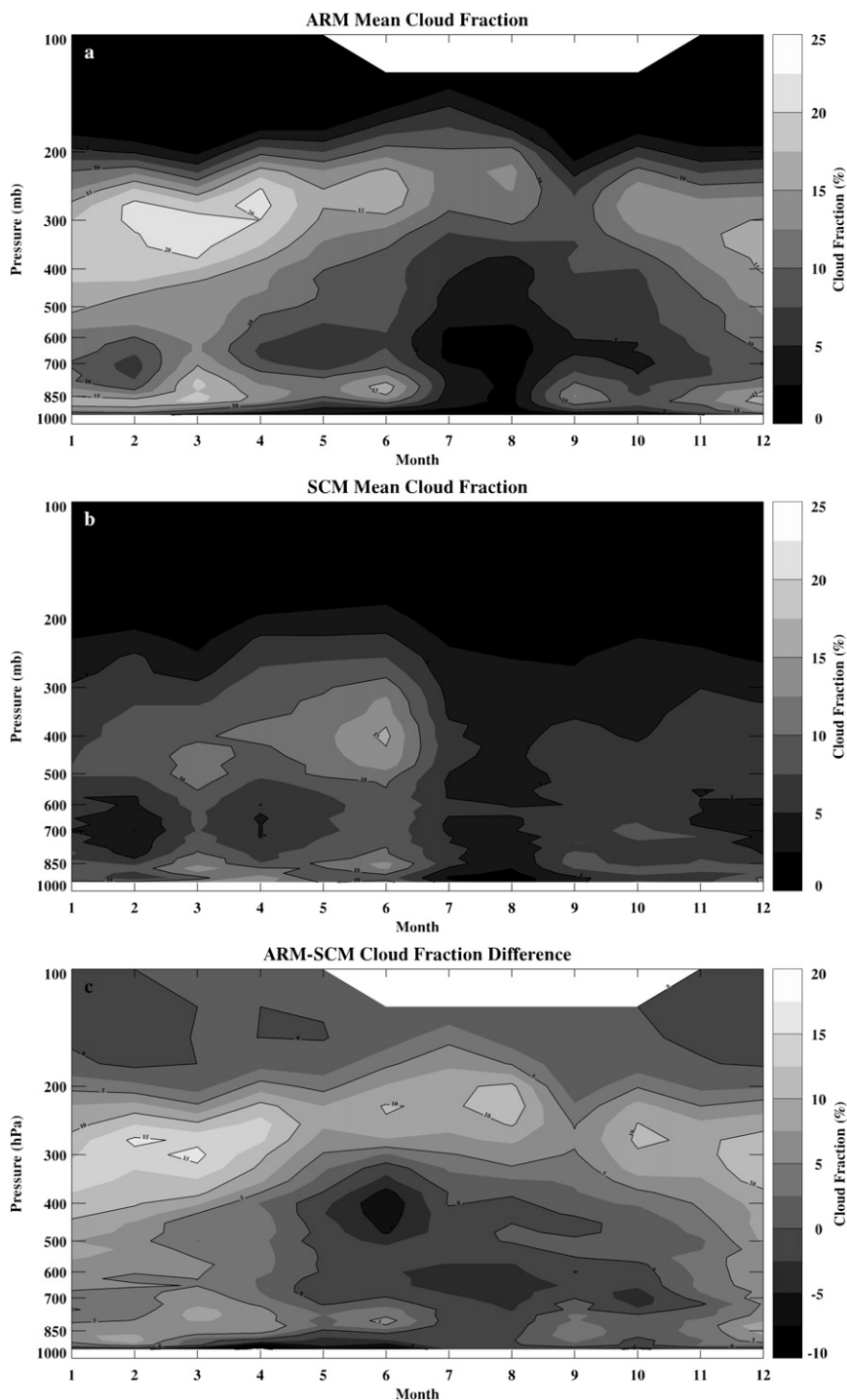


FIG. 6. Monthly mean cloud fraction during the period from 1999 to 2001 derived from (a) surface radar–lidar at ARM SGP and (b) the NASA GISS SCM model simulation and (c) the difference between the two mean cloud fractions.

clear or cloudy, and cloud fraction is not considered. To best represent the upper-level synoptic pattern, the 500-hPa geopotential height and vertical motion ($\omega < 0$ for upward and $\omega > 0$ for downward) and 300-hPa RH

were selected to study high clouds. For low clouds, mean sea level pressure (MSLP), 500-hPa ω , and 925-hPa RH were considered. These three parameters were then averaged for the following conditions: 1) periods when clouds

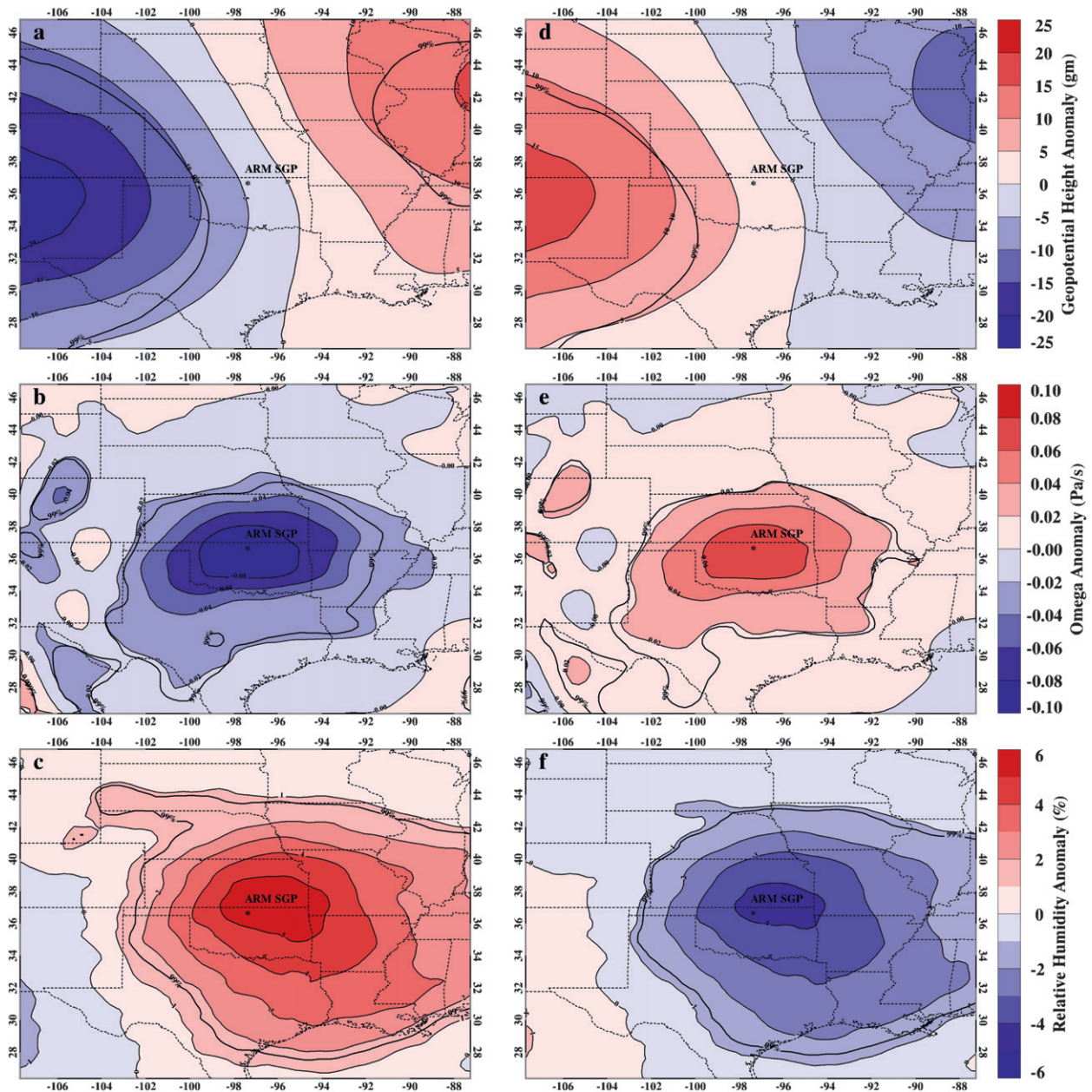


FIG. 7. The 500-hPa geopotential height, vertical velocity, and 300-hPa RH anomalies for time periods of correctly simulated (left) high cloud cover and (right) missed high cloud cover. The thicker black lines represent the 99% significance level.

were both observed and simulated (hit) and 2) clouds were observed but not simulated (miss). For brevity, these are referred to as hits and misses, although they are not quite the same as the more commonly used terminology that includes correct and incorrect simulations of null forecasts (no cloud).

a. High clouds

Figure 7 illustrates the 500-hPa geopotential height and vertical velocity and 300-hPa relative humidity anomalies

(relative to the 3-yr period) for both the modeled and missed high clouds over the SGP during the 3-yr period. The 500-hPa geopotential height field for model hits (Fig. 7a) is characterized by a dipole pattern with negative (positive) anomalies from climatology west (east) of the SGP. This is indicative of a trough upstream of the site for model hits. The maximum negative geopotential height anomalies are approximately 20 m below the climatological geopotential height of observed high clouds and are within the 99% significance level.

TABLE 3. Percentages of observed and modeled high clouds occurring during stratiform conditions ($\omega \geq 0$) at the 500-hPa level.

| | Year | Season | | | |
|---------|------|--------|-----|-----|-----|
| | | DJF | MAM | JJA | SON |
| OBS (%) | 36 | 33 | 32 | 47 | 36 |
| SCM (%) | 21 | 19 | 23 | 25 | 23 |

Model hits are also associated with strong upward motion in the ω field (Fig. 7b) and positive relative humidity anomalies (Fig. 7c). The entire model domain is easily within the 99% significance level with a peak vertical motion anomaly of -0.08 Pa s^{-1} and an RH anomaly of 5%.

Model misses are characterized by a reversal in the NARR fields, which nearly mirrors the synoptic pattern for model hits. Geopotential height anomalies are consistent (Fig. 7d) with a ridge to the west of the ARM SGP. Although this pattern is statistically significant, the amplitude (15 m) is less than that of the trough. Likewise, model misses are associated with sinking motion and drier conditions. These fields, while significant at the 99% level, have magnitudes of 0.06 Pa s^{-1} for ω and -4% for RH, less than those associated with the trough.

These results are consistent with the hypothesis that the model is primarily producing high clouds during synoptically evident events. High clouds are typically formed when a trough lies west of ARM SGP. From quasigeostrophic theory, one would expect rising motion to occur east of the trough axis and, with this rising motion, increased moisture transport to the upper troposphere. Model misses, however, occur when clouds are associated with a large-scale ridge. Associated with this ridge is sinking motion and negative RH anomalies. At least some of the missed high clouds can be explained through this analysis. When there are few baroclinic waves, simulated high clouds occur infrequently. This normally occurs over the SGP region during the summer months when the polar jet is shifted farther north. High clouds still occur frequently during the summer, however, which indicates these might occur due to subgrid-scale forcing, such as local thunderstorms. This argument is reinforced by the values in Table 3, which presents the percentage of high-cloud fraction that occurs during the periods of 500-hPa subsidence. Approximately one-third of the clouds satisfy this condition year round with the highest percentage (47%) occurring during the summer season. The percentages of modeled high clouds, however, are only $\sim 20\%$ – 25% (compared to the observed 32%–47% CF). By the very nature of the forcing that is constrained by precipitation, high clouds associated with convective cores should be associated with rising motion

in the column. High-cloud cover during time periods of neutral and sinking motion must be simulated by the stratiform parameterization. The low model percentages compared to observations suggest that the stratiform scheme is suspect in generating enough high-cloud cover. Is it possible for this parameterization within the SCM to accurately simulate a realistic amount of high cloud?

b. Low clouds

The relationships of low clouds with NARR fields are given in Fig. 8. Model hits are characterized by lower MSLP (Fig. 8a), weak rising motion (Fig. 8b), and positive RH anomalies (Fig. 8c). Although the patterns are similar to those for high clouds and significant at the 99% level, the magnitudes of these fields are much lower: 1 hPa, -0.01 Pa s^{-1} , and 4%. The weak relationship to 500-hPa vertical motion can be explained by low clouds being controlled by PBL processes. The weak relationship of low clouds with RH is somewhat surprising, however.

Anomalies for model misses are opposite to those for hits, but are much greater in magnitude. Values over the ARM SGP are 3 hPa for MSLP, 0.08 Pa s^{-1} for ω , and -14% for RH. While their patterns are asymmetric compared to those of high clouds, the most striking difference is the large difference in magnitude. To explain this difference and to also answer the questions raised for high clouds, it is necessary to examine the seasonal and vertical variations of clouds related to the RH and ω fields from both ARM forcing and the NARR datasets.

5. Relationships between clouds and large-scale parameters

In section 4, it was found that most of the missed clouds occurred during quiescent conditions with either neutral or sinking vertical motions and lower humidity values. Model biases may be due to the frequency of clouds that occur from subgrid-scale variability, the current stratiform RH threshold of $U_{00} = 60\%$ being unrepresentative of conditions at SGP, or errors in the forcing itself.

To answer these questions, PDFs are calculated for the following two relationships: (i) the probability of a given value of RH/ ω occurring for cloudy scenes and (ii) the probability of cloud occurrence for a given value of RH/ ω . Observed CF from the ARM SGP site is compared with area averages from ARM forcing and NARR at an equivalent resolution. Simulated clouds are compared with values from the driving ARM forcing.

a. Relationship of RH to high and low clouds

The probabilities of a given RH occurring for observed and modeled high cloud scenes are illustrated in Fig. 9a.

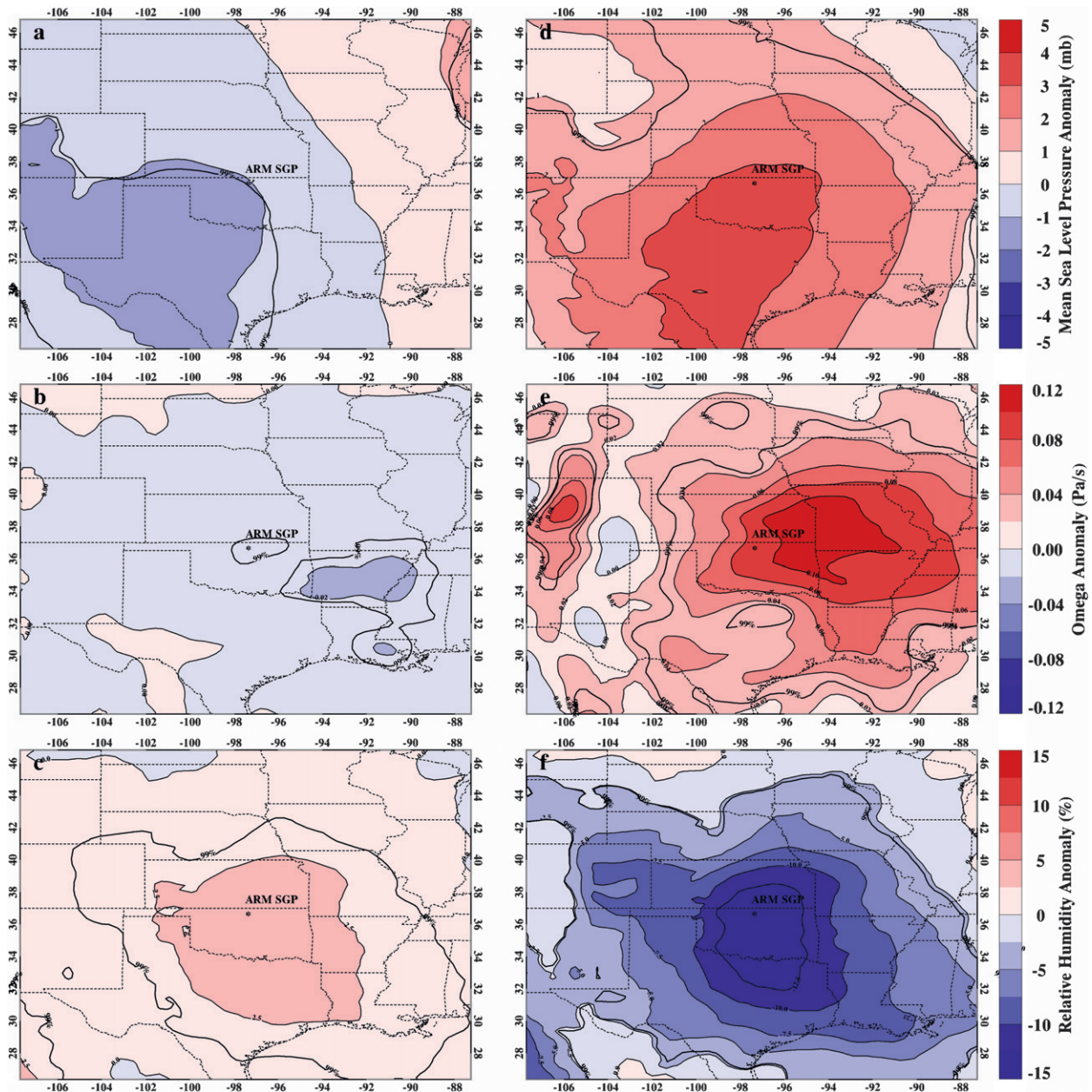


FIG. 8. MSLP, 500-hPa vertical velocity, and 925-hPa RH anomalies for time periods of (left) correctly simulated low cloud cover and (right) missed low cloud cover. The thicker black lines represent the 99% significance level.

The observed high clouds have near-Gaussian distributions with RH peaks occurring near 50% and 40% for ARM and NARR, respectively. The NARR distribution is narrower in width with higher probabilities than ARM. The model's peak is at $\sim 65\%$ – 70% RH for both total and stratiform cloud fractions. This is a function of the stratiform cloud parameterizations used in the model that limits cloud development below U_{00} . While not shown, the probability distribution functions of RH for all clear

and cloudy scenes show that the SCM produces higher RH and fewer low RH values than indicated by the continuous forcing and NARR at the SGP, suggesting either a shortcoming in the observations or an issue with the stratiform parameterization. Together, the tendency for high RH values and the parameterization specification that restricts stratiform cloud to high RH cause the probability of high cloud to increase nearly exponentially with RH, a feature not seen in the data (Fig. 9b).

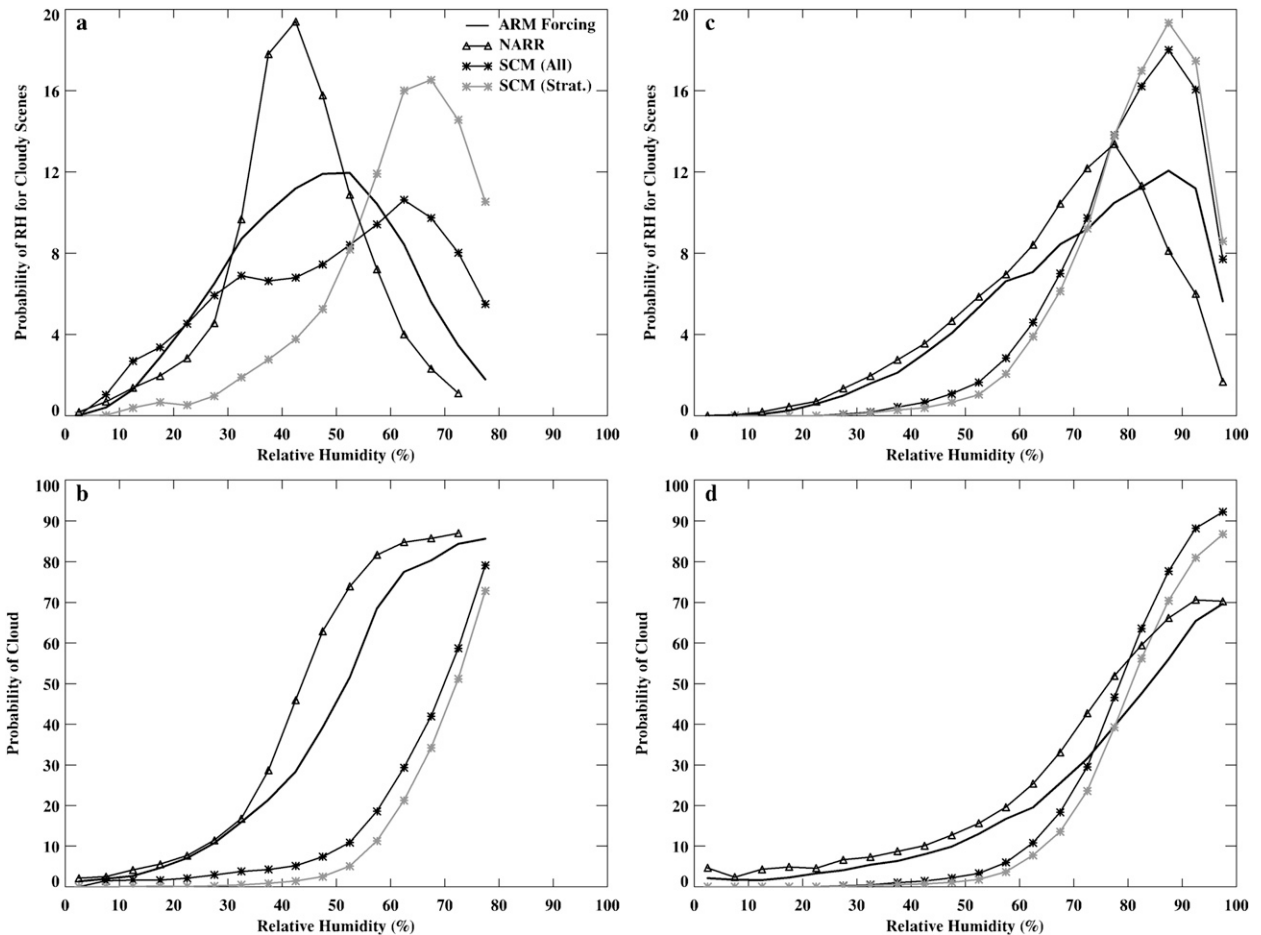


FIG. 9. Dependence of high and low cloud occurrences on RH (5% bins). Probabilities of (a) RH for observed and simulated high cloud scenes and (b) high cloud occurrence for a given RH. (c),(d) As in (a),(b) but for low clouds. Simulated clouds for total (black stars) and stratiform (gray stars) are compared to values from ARM forcing, while observed clouds are compared to both ARM and NARR. Note that data are only plotted for bins that contribute at least 0.05% to the total distribution.

For low clouds, several differences exist. The probabilities of RH for observed cloudy scenes (Fig. 9c) have gammalike distributions with peaks at 75%–85% RH and a sharp dropoff toward RH = 100%. The model histograms have similar shapes to the observed but with higher peak values and at a slightly higher RH than NARR. The PDF for RH occurrence (not shown) also has too many high RH values, as for high clouds, but is otherwise similar in shape to the observations. Unlike high clouds, the probability of observed low clouds occurring at high RH is much lower with only a 60% probability at RH values of 95%–100% (Fig. 9d). For the SCM, the cloud probability increases sharply with RH > 60%, consistent with the specified U_{00} . Because the majority of low clouds occur at high RH, there is little difference for the periods when clouds are both observed and simulated. Model misses, on the other hand, occur frequently

when low clouds occur at RH values well below the threshold.

b. Relationship of ω to high and low clouds

As was done for RH, PDFs for ω were also calculated and are shown in Fig. 10. Results for high and low clouds are similar in many regards. Compared to the ARM forcing, the NARR distribution is positively skewed with a noticeable tail at larger values of sinking motion between 5 and 20 mb h^{-1} . Reinforcing the results from section 4, the model has a negative bias compared to both ARM and NARR, producing the majority of its high clouds during times of rising motion (negative ω). Probabilities of high cloud in Fig. 10b drop significantly when vertical motion changes from upward to downward. While the PDFs derived from ARM forcing and NARR agree well for negative values of ω , NARR is asymptotic to a value $\sim 10\%$ higher than ARM. This

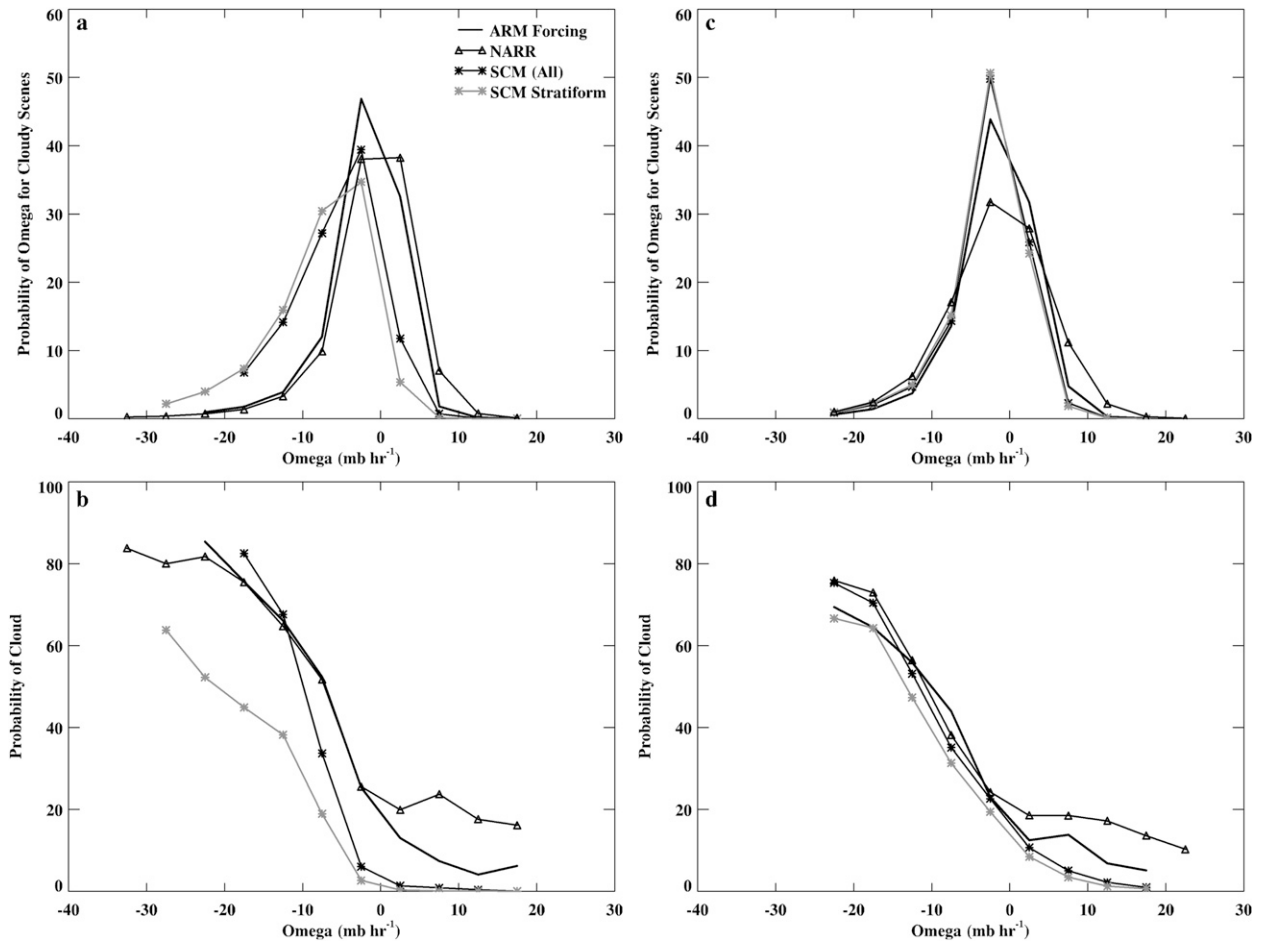


FIG. 10. As in Fig. 9 but for ω (5 mb h^{-1} bins).

feature is also noticeable for low clouds to a lesser extent. In the lower levels, the model predominantly produces stratiform clouds; hence, the two distributions for total and stratiform CF are nearly identical (Fig. 10c).

c. Discussion

The results from this section highlight the seasonal and vertical variations of clouds related to RH and ω . In the lower troposphere, a RH threshold of $U_{00} = 60\%$ captures the majority of low clouds and leads toward an overproduction (positive bias) of low clouds due to the amount of clear scenes that occur at $\text{RH} > 60\%$ in the lowest several model layers. For high clouds, many clouds are observed well below the SCM stratiform RH threshold U_{00} . If the model can only produce high clouds during the periods of upwelling motion or higher humidity in the upper troposphere, it is easily understood why the SCM has a negative bias for high clouds. The best balance occurs in the midlevels where the modeled cloud fraction is similar to both radar and satellite observations.

6. Summary and conclusions

The NASA GISS SCM simulated clouds over the ARM SGP have been compared with combined radar–lidar and satellite observations over the ARM SGP during the period 1999–2001. To qualitatively and quantitatively investigate how well the observed and modeled clouds were associated with large-scale synoptic patterns and variables, the observed and modeled clouds with ARM forcing and NARR data were explored. Through an integrative analysis of observations, simulations, and forcing/reanalysis datasets, the following conclusions are reached:

- 1) The GOES-derived total CFs from both 0.5° and 2.5° grid boxes are in excellent agreement with surface observations, which shows that ARM point observations can represent large areal observations on yearly and even monthly time scales at a relatively low level ($\sim 2\%$) of uncertainty at the ARM SGP. For individual cloud layers, the GOES-derived CFs are less

than the surface observations because of cloud overlap issues and the limitations of detecting clouds using passive satellite observations. Compared with the surface–GOES observations, the SCM simulates most of the midlevel clouds, overestimates low clouds (4%, in the lowest two layers), and underestimates total and high clouds by 7% and 15%, respectively. The most notable difference between observations and simulations is the lack of modeled high clouds regardless of season. There is no strong diurnal variation for both surface and GOES-derived total clouds. A significant drop for high clouds and a bump for both low and middle clouds around sunrise (~ 1200 – 1300 UTC) for GOES observations are mainly caused by the usage of two different retrieval algorithms for day and night.

- 2) Investigation of NARR data for the modeled high clouds reveals the model hit (missed) clouds occur during a trough (ridge) upstream of the ARM SGP. These synoptic patterns are associated with rising (sinking) motion and positive (negative) RH anomalies. Modeled clouds are associated with the rising motion that occurred over the east of the trough axis and increased moisture transport to the upper troposphere. The model misses, however, are associated with large-scale ridging, sinking motion, and negative RH anomalies. At least part of the missed high clouds can be explained through this analysis. Fewer high clouds can be produced during the periods when baroclinic wave activity is infrequent, a condition that normally occurs over the SGP region during summer months when the polar jet is shifted farther north.
- 3) The probability distributions of RH occurrence differ for observed high- and low-cloud scenes. High clouds have a Gaussian-like distribution with a peak at $\sim 40\%$ – 50% RH, whereas low clouds have a gammalike distribution with the highest cloud probability occurring at RH between 75% and 85%. While the distributions of observed and modeled low clouds are mostly similar to each other, the modeled high cloud distributions peak at greater RH values than the observations. The negative bias in the modeled high clouds is mainly caused by the SCM RH threshold because most observed clouds occur at RH values below what was specified for this run (60%). Although model results are qualitatively the same whether they are compared to ARM forcing or NARR, differences between these two datasets warrant further investigation.

The results presented in this study only represent clouds over a single continental area during the 3-yr

period. While the results study suggest some possible directions for improvement, similar analyses and tests need to be performed in other climate regimes, such as arctic, tropical, and subtropical ocean regions, to see whether the insights achieved are general or location specific. A variety of other questions remain unresolved. A large percentage of clouds over the ARM SGP are forced at scales unresolved by the continuous forcing. In particular, convection poses a significant challenge to GCM modelers. How feasible is it for any SCM to diagnose such clouds in the absence of knowledge about the forcing on smaller scales? It may be possible to gather additional statistics on these clouds by incorporating precipitation radars over the SGP site to give a complete picture about convective clouds, including their core and stratiform regions. Other questions related to the cloud microphysical and optical properties and their impact on the surface and TOA radiation budget are also important. Until these questions are explored in detail, it is impossible to understand the true validity of the NASA GISS GCM/SCM and its cloud parameterizations.

Acknowledgments. The authors thank a variety of individuals and organizations. Anonymous reviewers provided many helpful suggestions that led to a more concise and complete manuscript. The SGP continuous forcing dataset was kindly supplied by Shaocheng Xie and the ARM program. NARR reanalysis data were provided by NOAA/OAR/ESRL PSD, Boulder, Colorado, from their Web site at (<http://www.esrl.noaa.gov/psd/>). This research was primarily supported by the NASA MAP project under Grant NNG06GB59G at the University of North Dakota. The first author was also supported by the North Dakota Space Grant Consortium fellowship. The University of North Dakota authors were also supported by the NASA CERES project under Grant NNL04AA11G, the NASA NEWS project under Grant NNX07AW05G, and NSF under Grant ATM0649549.

REFERENCES

- Ackerman, T. P., and G. M. Stokes, 2003: The Atmospheric Radiation Measurement Program. *Phys. Today*, **56**, 38–44.
- Benjamin, S. G., and Coauthors, 2004: An hourly assimilation/forecast cycle: The RUC. *Mon. Wea. Rev.*, **132**, 495–518.
- Cess, R. D., and Coauthors, 1996: Cloud feedback in atmospheric general circulation models: An update. *J. Geophys. Res.*, **101** (D8), 12 791–12 794.
- Clothiaux, E. E., T. P. Ackerman, G. G. Mace, K. P. Moran, R. T. Marchand, M. A. Miller, and B. E. Martner, 2000: Objective determination of cloud heights and radar reflectivities using a combination of active remote sensors at the ARM CART sites. *J. Appl. Meteor.*, **39**, 645–665.

- Del Genio, A. D., and M.-S. Yao, 1993: Efficient cumulus parameterization for long-term climate studies: The GISS scheme. *The Representation of Cumulus Convection in Numerical Models*, Meteor. Monogr., No. 46, Amer. Meteor. Soc., 181–184.
- , W. Kovari, and K. K. W. Lo, 1996: A prognostic cloud water parameterization for global climate models. *J. Climate*, **9**, 270–304.
- , W. Kovari, M.-S. Yao, and J. Jonas, 2005a: Cumulus microphysics and climate sensitivity. *J. Climate*, **18**, 2376–2387.
- , A. B. Wolf, and M.-S. Yao, 2005b: Evaluation of regional cloud feedbacks using single-column models. *J. Geophys. Res.*, **110**, D15S13, doi:10.1029/2004JD005011.
- Dong, X., B. Xi, and P. Minnis, 2006: A climatology of mid-latitude continental clouds from the ARM SGP Central Facility. Part II: Cloud fraction and surface radiative forcing. *J. Climate*, **19**, 1765–1783.
- , P. Minnis, B. Xi, S. Sun-Mack, and Y. Chen, 2008: Comparison of CERES-MODIS stratus cloud properties using ground-based measurements at the DOE ARM SGP site. *J. Geophys. Res.*, **113**, D03204, doi:10.1029/2007JD008438.
- Gao, S., and X. Li, 2007: *Cloud-Resolving Modeling of Convective Processes*. Springer, 206 pp.
- Hogan, R. J., C. Jakob, and A. J. Illingworth, 2001: Comparison of ECMWF winter-season cloud fraction with radar-derived values. *J. Applied Meteor.*, **40**, 513–525.
- Klein, S. A., and C. Jakob, 1999: Validation and sensitivities of frontal clouds simulated by the ECMWF model. *Mon. Wea. Rev.*, **127**, 2514–2531.
- , and A. D. Del Genio, 2006: ARM's support for GCM improvement: A white paper. UCRL-MI-224010, ARM-06-012.
- Mesinger, F., and Coauthors, 2006: North American Regional Reanalysis. *Bull. Amer. Meteor. Soc.*, **87**, 343–360.
- Min, Q., P. Minnis, and M. M. Khaiyer, 2004: Comparison of cirrus optical depths from GOES-8 and surface measurements. *J. Geophys. Res.*, **109**, D20119, doi:10.1029/2003JD004390.
- Minnis, P., W. L. Smith Jr., D. P. Garber, J. K. Ayers, and D. R. Doelling, 1995: Cloud properties derived from GOES-7 for the spring 1994 ARM intensive observing period using version 1.0.0 of the ARM satellite data analysis program. NASA Ref. Publ. 1366, 59 pp.
- , and Coauthors, 2001: A near-real time method for deriving cloud and radiation properties from satellites for weather and climate studies. Preprints, *11th Conf. on Satellite Meteorology and Oceanography*, Madison, WI, Amer. Meteor. Soc., 477–480.
- , and Coauthors, 2008: Cloud detection in non-polar regions for CERES using TRMM VIRS and Terra and Aqua MODIS data. *IEEE Trans. Geosci. Remote Sens.*, **46**, 3857–3884.
- Moran, K. P., B. E. Martner, M. J. Post, R. A. Kropfli, D. C. Welsh, and K. B. Widener, 1998: An unattended cloud-profiling radar for use in climate research. *Bull. Amer. Meteor. Soc.*, **79**, 443–455.
- Palikonda, R., and Coauthors, 2006: NASA-Langley Web-based operational real-time cloud retrieval products from geostationary satellites. *Remote Sensing of the Atmosphere and Clouds*, S.-C. Tsay, T. Nakajima, and R. P. Singh, Eds., International Society for Optical Engineering (SPIE Proceedings, Vol. 6408), doi:10.1117/12.700423.
- Randall, D. A., K. M. Xu, R. J. Somerville, and S. Iacobellis, 1996: Single-column models and cloud ensemble models as links between observations and climate models. *J. Climate*, **9**, 1683–1697.
- , M. E. Schlesinger, V. Galin, V. Meleshko, J.-J. Morcrette, and R. Wetherald, 2006: Cloud feedbacks. *Frontiers in the Science of Climate Modeling*, J. T. Kiehl and V. Ramanathan, Eds., Cambridge University Press, 217–250.
- Rossow, W. B., and R. A. Schiffer, 1999: Advances in understanding clouds from ISCCP. *Bull. Amer. Meteor. Soc.*, **80**, 2261–2287.
- Smith, W. L., P. Minnis, H. Finney, R. Palikonda, and M. M. Khaiyer, 2008: An evaluation of operational GOES-derived single-layer cloud top heights with ARSCL over the ARM Southern Great Plains site. *Geophys. Res. Lett.*, **35**, L13820, doi:10.1029/2008GL034275.
- Sundqvist, H., E. Berge, and J. E. Kristjánsson, 1989: Condensation and cloud parameterization studies with a mesoscale numerical weather prediction model. *Mon. Wea. Rev.*, **117**, 1641–1657.
- Warren, S. G., C. J. Hahn, J. London, R. M. Chervin, and R. L. Jenne, 1984: Atlas of simultaneous occurrence of different cloud types over land. NCAR Tech. Note NCAR/TN-241+STR, 209 pp.
- Wielicki, B. A., and Coauthors, 1996: Clouds and the Earth's Radiant Energy System (CERES): An Earth Observing System experiment. *Bull. Amer. Meteor. Soc.*, **77**, 853–868.
- Xi, B., X. Dong, P. Minnis, and M. Khaiyer, 2010: A 10-year climatology of cloud fraction and vertical distribution derived from both surface and GOES observations over the DOE ARM SGP Site. *J. Geophys. Res.*, **115**, D12124, doi:10.1029/2009JD012800.
- Xie, S., R. T. Cederwall, and M. Zhang, 2004: Developing long-term single-column model/cloud system-resolving model forcing data using numerical weather prediction products constrained by surface and top of the atmosphere observations. *J. Geophys. Res.*, **109**, D01104, doi:10.1029/2003JD004045.
- Zhang, G. J., 2003: Lagrangian study of cloud properties and their relationships to meteorological parameters over the U.S. Southern Great Plains. *J. Climate*, **16**, 2700–2716.
- Zhang, M. H., J. L. Lin, R. T. Cederwall, J. J. Yio, and S. C. Xie, 2001: Objective analysis of ARM IOP data: Method and sensitivity. *Mon. Wea. Rev.*, **129**, 295–311.
- Zhang, M. J., and Coauthors, 2005: Comparing clouds and their seasonal variations in 10 atmospheric general circulation models with satellite measurements. *J. Geophys. Res.*, **110**, D15S02, doi:10.1029/2004JD005021.